INTERNATIONAL JOURNAL OF SMART AND NANO MATERIALS
2022, VOL. 13, NO. 2, 330–345
https://doi.org/10.1080/19475411.2022.2084172

Influence of thermal treatment on electronic properties of inkjet-printed zinc oxide semiconductor

Van-Thai Tran [a], Yuefan Wei [b] and Hejun Du [a,c]

[a]Singapore Centre for 3D Printing, Nanyang Technological University, Singapore; [b]Advanced Remanufacturing and Technology Centre, Singapore; [c]School of Mechanical and Aerospace Engineering, Nanyang Technological University, Singapore

ABSTRACT

Additive manufacturing of electronic devices using inkjet printing provides a potential alternative approach in substitution for conventional electronic fabrication processes. However, the complex nature of inkjet printing involves the liquid deposition and film formation from the vaporization of solvent, which makes it different from film created by conventional deposition methods. Inkjet printing of zinc oxide (ZnO), which is a widely utilized semiconductor, produces polycrystalline film composed of nano-size grains, which could significantly influence the properties of printed film. In this study, low-temperature annealing was employed to treat inkjet-printed ZnO for UV photodetection application, and its influence on electrical properties was studied. Band bending was characterized using the Mott-Schottky plot which examines the charge distribution of the films. It is found that the annealing of inkjet-printed polycrystalline ZnO film has improved its electrical properties, which could be attributed to the reduction of band bending due to the merging of grains. The treatment also helps to reduce impurities of the film, such as zinc hydroxide complexes, which is common for solution-derived films. Hence, the study could pay the way for the improvement of electrical properties of inkjet-printed functional materials.

ARTICLE HISTORY
Received 2 April 2022
Accepted 23 May 2022

KEYWORDS
Inkjet printing; zinc oxide; electrical properties; band bending; thermal annealing

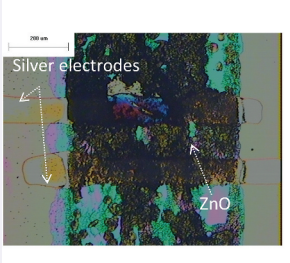

Inkjet-printed ZnO

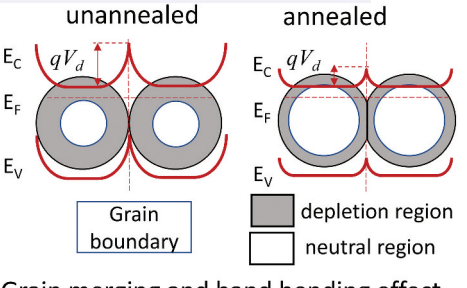

Grain merging and band bending effect

CONTACT Hejun Du MHDU@ntu.edu.sg Singapore Centre for 3D Printing, Nanyang Technological University, Singapore; Advanced Remanufacturing and Technology Centre, Singapore; School of Mechanical and Aerospace Engineering, Nanyang Technological University, Singapore

The manuscript was written through contributions of all authors. All authors have given approval to the final version of the manuscript.

1. Introduction

Printing of functional material could promote the application of electronic devices via additive manufacturing approaches, whereby the material is gradually deposited to form the desired physical structure from a digital design [1,2]. Among different additive manufacturing technologies, inkjet printing is one of the most suitable techniques for electronic printing thanks to its merits such as non-contact deposition, high precision, being capable of printing multiple materials, and being compatible with flexible substrates [3]. Printing of conductive materials, which are the fundamental of electronic printing, have been extensively explored, such as the printing of silver nanoparticle to create conductive patterns [4]. These printings were conducted on flexible substrates such as polymer substrates, which demonstrated the feasibility of flexible electronic manufacturing by additive manufacturing [5,6]. Considerably, printing of transparent conductive film is possible, which widen the capability of additive manufacturing [7]. Beside conventional transparent electrode material such as indium-tin-oxide-based, printing in large-area of transparent conductive film could be implemented by alternative inks such as silver nanoparticles [8], conductive polymer [9,10]. Furthermore, the printing of different materials with specific functionality could construct devices with performance comparable to conventional fabrication approaches [11–13].

ZnO is an attractive wide bandgap semiconductor that has gathered a vast interest in various optoelectronic applications, such as transistors [14,15], photodetectors [16,17], and solar cells [18,19]. Recent developments of ZnO-based device witness the employment of this multi-functionals material on a rapid immunoassay test for SARS-CoV-2 virus [20].

Hence, ZnO nanostructures, such as nanowires and nanoparticles [21,22], have been an attractive source for various effort in inkjet printing of semiconductor materials for construction of functional devices.

Noticeably, the characteristics of the printed material determine the performance of the fabricated device. Because the polycrystalline structure is the main feature of the inkjet-printed ZnO, the grain boundaries have a major effect on electron transportation via the band bending at the grain interface [23,24]. It is well known that the electrical characteristics engineering of polycrystalline semiconductors could be achieved by modification of grain boundary as proven by previous studies [25,26]. For example, nano junction was adjusted to control band bending and enhance the efficiency of photosensing [27]. The band bending was also be tuned by rapid thermal treatment to obtain enhanced optoelectrical performance [28]. Notably, low temperature annealing of ZnO has been investigated using laser treatment to promote the coalescence of the ZnO nanoparticle [29,30]. Therefore, engineering the electronic properties of inkjet-printed ZnO is possible via modification of band bending.

In this work, the engineering of inkjet-printed ZnO electrical properties using relatively low annealing temperatures was studied. The photosensitivity of printed UV photodetector exhibits a strong dependence on annealing temperature, such as the higher the temperature, the higher photocurrent. The increment of photocurrent was attributed to the reduction of the flat band potential of printed ZnO thin film as a result of thermal annealing. Surface states were studied using X-ray photoelectron spectroscopy (XPS), which is linked to the response characteristics of photocurrent under UV illumination. This

work presents a simple method for the treatment of inkjet-printed ZnO thin film for optoelectronic application by relatively low-temperature annealing. The treatment helps reducing impurities of inkjet-printed ZnO film, such as zinc hydroxide complexes [31]. The significance of band bending to the characteristics of inkjet-printed UV sensor is also demonstrated, and a higher responsivity could be achieved by reducing band bending of the inkjet-printed semiconductor thin film.

2. Materials and methods

2.1. Inkjet printing and formation of ZnO from zinc precursor

Zinc acetate dihydrate solution in ethanol with a concentration of 50 mM was employed as the ink for printing of zinc precursor in the process published in our previous report [16]. A commercial inkjet printer (Dimatix 2831, Fujifilm) was employed for the printing. For fabrication of UV photodetector, both the semiconductor, i.e. ZnO, and conductor, i.e. silver, were printed on Si/SiO_2 substrate. Firstly, two silver patterns were printed to create the electrodes for the device. These silver electrodes are annealed at 150°C to sinter the nanoparticles and improve their conductivity. The silver electrodes are about 100 µm in width, and the space between the two electrodes is 110 µm by 600 µm, which are later covered by the ZnO thin film to form the UV photodetector structure. The zinc salt was printed on top of the silver electrodes to subsequently create metal-semiconductor junctions. The printed zinc salt was then undergone a heating step on a hotplate for 10 minutes at 200°C to form ZnO polycrystalline thin film via the thermal decomposing of the zinc precursor. The printed films were then annealed in a quartz tube furnace (Thermo scientific) for haft an hour at various temperatures from 250°C to 350°C to further improve the film quality.

2.2. Characterization

Field emission scanning electron microscope (FE-SEM, JEOL 7600) and transmission electron microscope (TEM, JEOL-JEM 2010) were employed to study the printed ZnO thin film surface structure. The crystallite size was quantified using an X-ray diffractometer (XRD, PANalytical Empyrean), which is equipped with a 0.154 nm CuKα radiation. Surface states of the printed film were studied using X-ray photoelectron spectroscopy (XPS, Kratos Analytical), which has source is a K-alpha X-rays of aluminum with photon energy of 1486.6 eV.

The electrical characteristics of the printed device were characterized using a source measure unit (SMU B2902A, Agilent) to provide a bias voltage of 5 V and measure the current running through the sensor. Optoelectrical performance was studied by illuminating the device with 365 nm UV light filtered from a xenon arc lamp source, the illumination power was 1.08 mW/cm^2. The wide wavelength provided by the xenon arc lamp was filted by a bandpass filter to obtain 365 nm wavelength only. The transition between light and dark conditions was triggered by a homemade mechanical shutter.

Mott-Schottky plots, which characterize the charge distribution of films, were employed to study the band bending property of the film via flat band potential values. The working electrodes were prepared by printing square patterns of ZnO film with an

exposing area of 100 mm^2 on ITO-coated glass. A platinum plate was used as the counter electrode, while silver/silver chloride was used as the reference electrode. All electrodes were immersed in Na_2SO_4 electrolyte solution (0.5 M) for the measurement. A potentiostat (CHI 760D, CH Instrument) was used to measure the impedance of the film versus applied potential with a frequency fixed at 463 Hz.

3. Results and discussion

3.1. Morphology and grain structure of the printed film

Printed ZnO thin films exhibit wrinkle surfaces as shown in (Figure 1(a-b)). The crumple structure might be the result of internal stress during the formation of film by thermal decomposition, which is widely observed in solution-derived thin film [32,33]. The wrinkle structures may increase the surface area of the device, hence increase the interaction with surrounding environment. Because of the involvement of air interaction to the UV photodetector response to UV radiation, the wrinkle surface mean that there is more area to interact with air and it will affect to the device performance. Furthermore, the

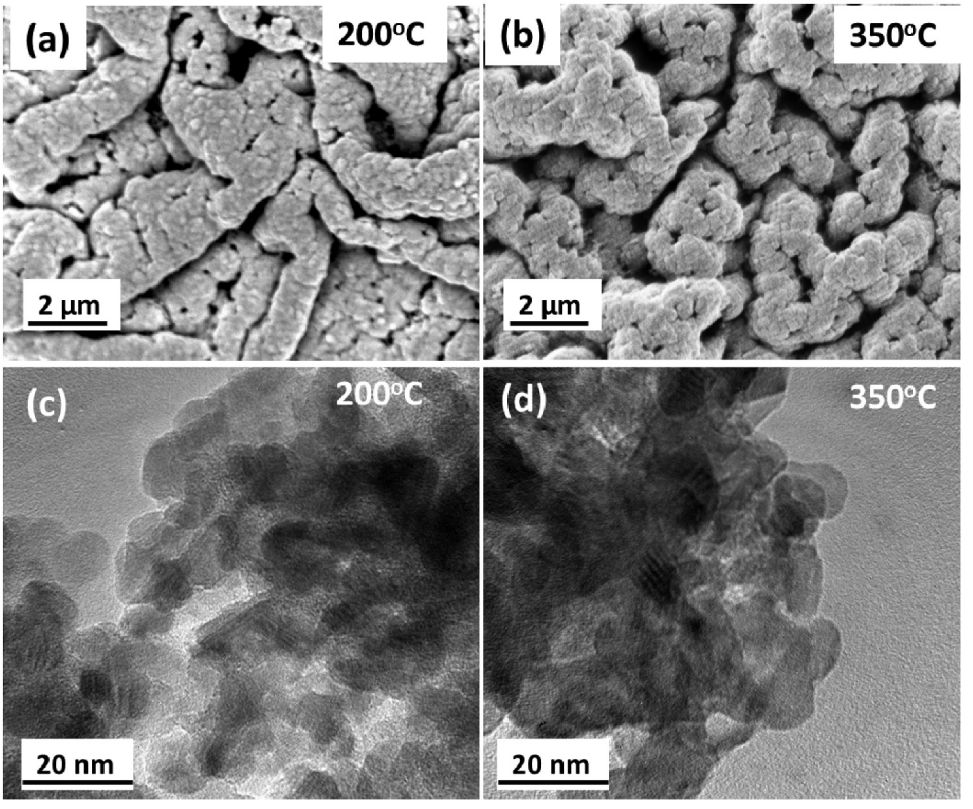

Figure 1. Morphology of printed ZnO films (a) with pre-heat treatment at 200°C and (b) with annealing at 350°C. Nanostructure of the film: (c) with pre-heat treatment at 200°C and (d) with annealing at 350°C.

wrinkle structures may improve more light absorbance, and lead to a higher efficiency of the device. For example, photovoltaic efficiency of solar cells was proven to be enhanced thanks to the winkle surface [34].

TEM image (Figure 1(c-d)) reveals that printed ZnO films have a polycrystalline structure composed of small grain with an estimated size smaller than 10 nm. However, there is no significant difference in the surface structure that could be observed between films with and without thermal annealing from these electron microscopic images.

The cross-sectional image of the ZnO thin films are shown in (Figure 2), which are clearly demonstrate the structure of the crumple films, composing of wrinkles due to thermal stress during the film processing. It is worth noting that general thickness of the film, which is about 2 μm (Figure 2(a-b)). However, it is in fact the height of the wrinkle film. The enlarge microscopic images show that the actual film thickness is about 200 nm only (Figure 2(c-d)).

To study the film structure, the crystallite size was quantified by XRD analysis, as shown in Figure 3. Representative peaks of ZnO with wurtzite crystal (JCPDS no. 36–1451), i.e. (100), (002), and (101), are located at $2\theta = 31.8\,°$, $34.4\,°$, and $36.3\,°$, respectively, could be identified for all of the samples [35]. These broad peaks can be attributed to the polycrystalline form of the printed ZnO thin films, which have a small crystallite size of a few nanometers. While the peak (002) has a relatively stable full width at half maximum (FWHM) value of about 1.4° which corresponds to a crystallite size that slightly varies around 6.1 nm, those of other peaks show a noticeable decrease, such as the peak (101)

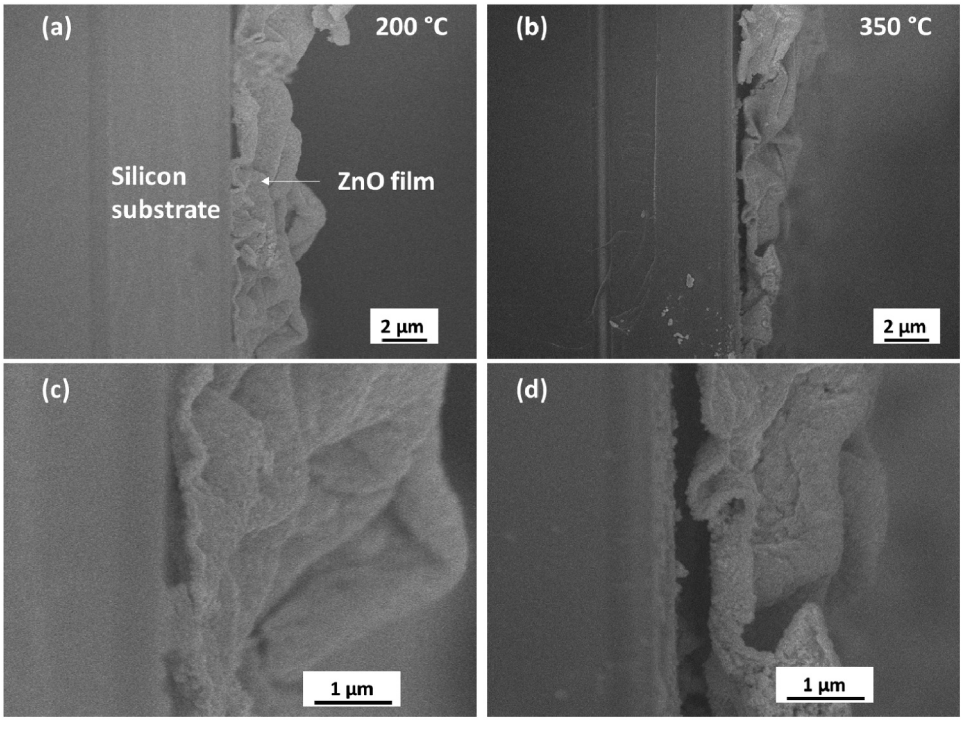

Figure 2. Cross-sectional image of the printed ZnO thin film, (a)- (c): with pre-heat treatment at 200°C and (b)- (d): with annealing at 350°C.

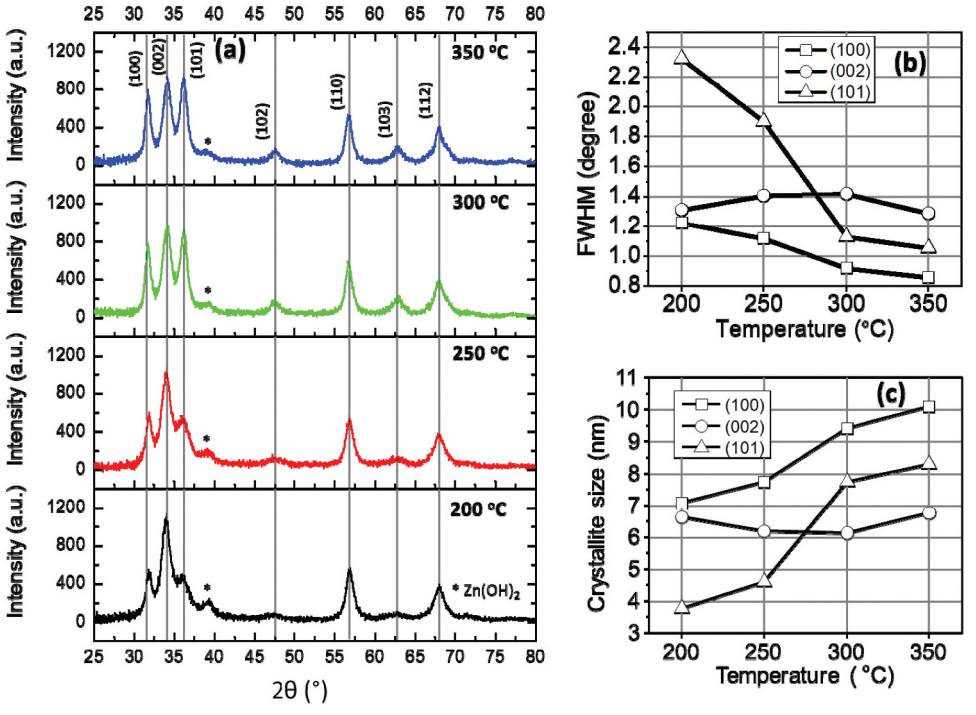

Figure 3. (a) XRD scanning result of films with different heat treatments. (b) Main peaks analysis by FWHM. (c) Crystallite sizes estimation from FWHM.

has FWHM value changing from 2.3° to 1.0°. This peak width reduction could be attributed to the increase in size along the peak, from 3.8 nm to 8.3 nm according to Scherrer's equation [36]. These results demonstrate that the annealing has promoted the merging of grains, which results in slightly larger grains of the annealed film. Furthermore, residual $Zn(OH)_2$ may be identified by the peak located at 39° [37]. Under the effect of thermal annealing, this peak intensity tends to reduce, which is evidence for the transformation from the residual to ZnO [38].

Along with annealing temperatures increasing, there was a change of film structure in term of crystal preferred orientation. It could be observed via the ratio of peak intensity of the axis (002) over the axis (100). While that ratio of the film with treatment at 200°C is about 2.2, the film with treatment at 350°C has a (002)/(100) ratio of 1.3. This means the film tends to transform from slightly c-axis preferred orientation to random orientation, which suggest the growth of crystal in other direction rather than (002).

3.2. Electrical properties

The electrical properties of the printed ZnO sensor were characterized by applying a bias voltage of 5 V and measuring the current under dark and UV illumination, and the result is plotted in (Figure 4(a-b)). It could be noticed that the electrical properties of printed ZnO are strongly affected by annealing conditions, such as the current under dark and UV

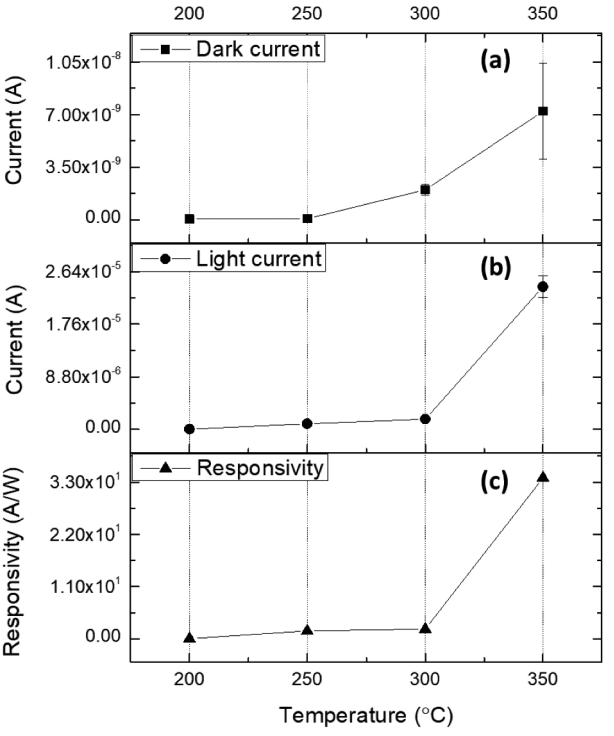

Figure 4. Electrical properties of printed ZnO measured at 5 V bias voltage: (a) electrical current under dark and (b) light illumination, (c) responsivity.

illumination increasing with the increase of annealing temperature. By annealing the film at 350°C, the dark current had raised 78 times, from 3.86×10^{-11} A to 3.03 x10^{-9}; and the photocurrent had notably raised 1386 times, from 1.89×10^{-8} A to 2.62×10^{-5} A.

Interaction of semiconductor lattice with photons that have energy equal to or larger than the bandgap of the semiconductor generates electron-hole pairs. These photon-generated charge carriers increase the charge concentration in the semiconductor film and lead to a surge of photocurrent. To evaluate the efficiency of the conversion from light to electrical current, the responsivity of the device under UV illumination is calculated by the ratio of photocurrent, J_{ph}, with light intensity P and illuminating area S [26]:

$$R = \frac{Jph}{PS} \tag{1}$$

The responsivity of printed sensors with different heat annealing temperatures is given in (Figure 4(c)), which shows that the responsivity has increased from 2.5×10^{-2} A/W to 33.9 A/W, which is over one thousand times. Hence, it could be concluded that the thermal annealing indeed improved the responsivity of the printed ZnO UV photodetector, which could be attributed to the improvement of electron transportation in the film.

The specific detectivity was calculated by $D^* = R/(2e\ I_{dark}/S)^{1/2}$ [26], where e is the absorlute value of electron charge, and the value for sample 200°C, 250°C, 300°C and 350°C are 1.86x10^{11}, 8.67x10^{12}, 2.87×10^{12} and 2.91x10^{13}, respectively. The external quantum efficiency (EQE) was calculated by $EQE = 124000I_{ph}/(\lambda P)$ [39], where I_{ph} is the

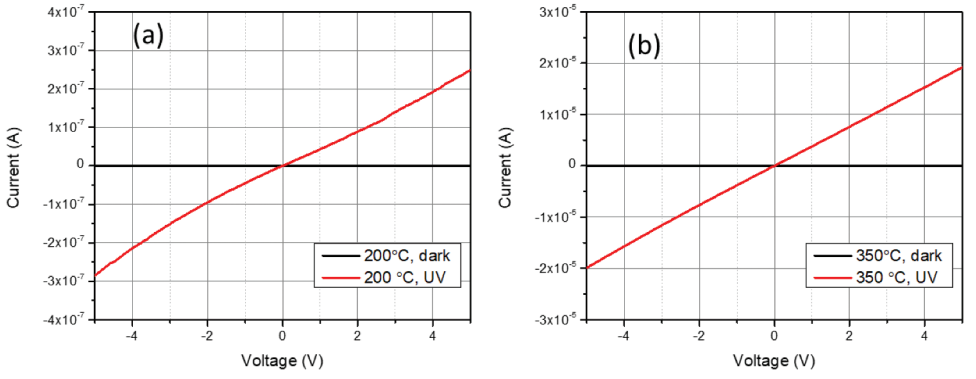

Figure 5. I–V characterisitcs of the printed UV photodetectors: (a) with preheat at 200°C and (b) with annealing at 350°C.

photocurrent density. It is found that the EQE of sample 200°C, 250°C, 300°C and 350°C are 8.33%, 574.4%, 694.5% and 11,522.7%, respectively. The results demonstrate that the thermal annealing indeed improves the performance of the printed UV photodetector.

The I–V characteristic of inkjet-printed ZnO UV photodetectors are shown in (Figure 5). It can be seen that the device with only pre-heat treatment at 200°C (Figure 5(a)) exhibits a nearly straight curve. On the other hand, the device with annealing at 350°C shows a linear I–V characteristics, which is the Ohmic property of the semiconductor-conductor contact (Figure 5(b)). This could be the result of thermal annealing which has helped improve the contact between ZnO film and silver electrodes.

Analytically, the conductivity of semiconductor film containing small grains could be expressed as [40]:

$$\sigma_d = \frac{q^2 N_d d}{(2\pi m * kT)^{1/2}} \exp(-qV_d/kT) \tag{2}$$

where q *is the electronic charge*, N_d *is the free carrier concentration*, d *is the crystallite size*, m* *is the effective electron mass and* V_d *is the potential barrier between the grains. Therefore, crystallite size and charge concentration are directly proportional to the conductivity of the film, while it is an exponential decay with barrier voltage. Further investigation on these parameters will be discussed to understand the mechanism of improved responsivity of annealed Z*nO.

3 nO.

3. Band bending study

Band bending at the grain boundary was characterized by impedance analysis to study the charge distribution at the film surface. By applying a potential between the ZnO thin film and the counter electrode, band bending level could be adjusted, and the applied value where the band bending is suppressed is the flat band potential, V_{fb} [41]. In this work, the flat band potential value is employed to study the band bending of the printed film.

The capacitance of the depletion layer could be adjusted by applying a potential between the ZnO film, which is the working electrode, and the counter electrode. The relationship between the capacitance, *C*, and the potential, *V*, could be described by the Mott-Schottky equation [42]:

$$\frac{1}{C^2} = \frac{2}{eN_dA^2\varepsilon\varepsilon_0}\left(V - V_{fb} - \frac{kT}{e}\right) \tag{3}$$

where *A* is the working electrode exposing area, N_d is the carrier concentration of the crystal, *k* is the Boltzmann constant, and the thermal voltage at room temperature, i.e. *kT/e*, could be found at 0.0257 V.

The Mott-Schottky analysis is shown in (Figure 6), which plots the value of $1/C^2$ by the potential, with a conventional resistance-capacitance model is employed [43]. From the plot, the fitted linear section intercepts with the horizontal axis at a value of *V*. Then, the flat band potential of each sample could be determined using the equation $V_{fb} = V\text{-}kT/e$. It could be seen that the magnitude of flat band potential of ZnO thin film reduces when thermal annealing was applied, such as the sample with only 200°C treatment has the flat band potential of −0.43 V, as compared to −0.11 V of the film with annealing at 350°C. This reduction in the magnitude of the flat band potential is evidence that band bending has been reduced by thermal annealing.

In addition, the slope of linear fitting, *m*, could be determined from the plot, and carrier concentration could be estimated by $N_d = 2/(meA^2\varepsilon\varepsilon_0)$ [42]. It is found that the concentration values of the films have slightly increased when annealing was applied, such as from 3.37×10^{20} cm^{-3} of the sample with 200°C treatment to 4.23×10^{20} cm^{-3} of the sample with 350°C treatment. These values are comparable to those of the nanoflower ZnO as reported by Allagui et al. [43].

Furthermore, the depletion layer width could be determined by $D = (A\varepsilon\varepsilon_0)/C$. At 0 V potential, the depletion width witnesses a reduction from 0.82 nm to 0.43 nm when applying thermal annealing. The reduction of the depletion layer means that there is less barrier between the grains, and therefore electrons can be transported through the boundaries easier.

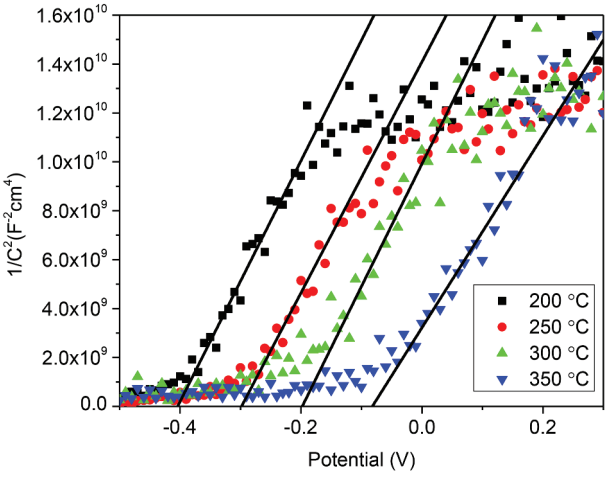

Figure 6. Mott-Schottky plots of the films with different annealing temperatures.

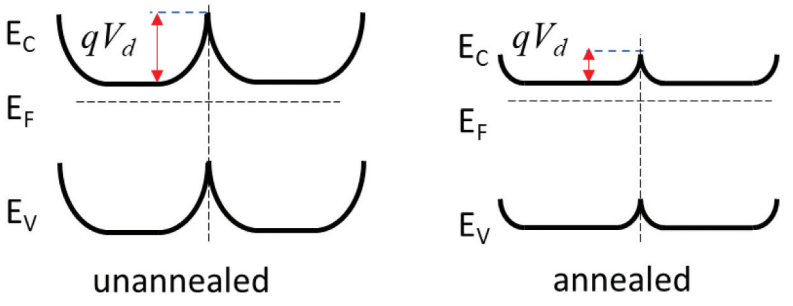

Figure 7. Energy diagram shows a reduction of band bending by grains merging.

3.4. Film conductivity by band bending effect

From the previous discussion, the conductivity of the film is proportional to crystallite size and charge concentration, which are both slightly increase by the thermal annealing. Hence, they would have a minor effect on the conductivity. However, it could be seen that the conductivity increases significantly, which might be mainly due to the influence of band bending reduction. An illustration of this mechanism is shown in (Figure 7), whereby the film is assumed to be a series of grains connected at the grain boundaries. Band bending at the grain boundaries tends to resist electron transportation through the film. Flat band potential analysis shows that film annealed at a higher temperature exhibits a lower band bending magnitude, which might be the result of the merging of grain boundary as suggested by the XRD analysis.

Furthermore, XRD analysis also suggests that there is a transformation from the residual to ZnO under the effect of heat treatment. Those residual defects could play the role of recombination centers, where photo-generated electrons are recombined with holes which reduces the carrier concentration in the printed film [44,45]. Hence, decreasing the residual could prolong the lifetime of photo-generated electrons and improve the photocurrent, as can be observed in the annealed sample.

3.5. Dynamic response of the printed sensor to UV illumination

When the sensor was exposed to UV light, the electrical current raised until it reaches the maximum value. When the UV light was removed, the current gradually decays to the original value. These dynamic responses are presented in (Figure 8(a)). The rise time and fall time of the response are defined by the time the signal raises from 10% to 90% and vice versa. The rise time of samples processed at 200°C, 250°C, 300°C and 350°C are 18.9 s, 55.6 s, 14.1 s and 43.1 s, respectively. The fall time of these samples are 15.1 s, 80.6 s, 47.7 s and 157.8 s, respectively. It can be seen that there is a general trend of increasing reaction time of the sample processed with higher temperature, except for the sample at 250°C.

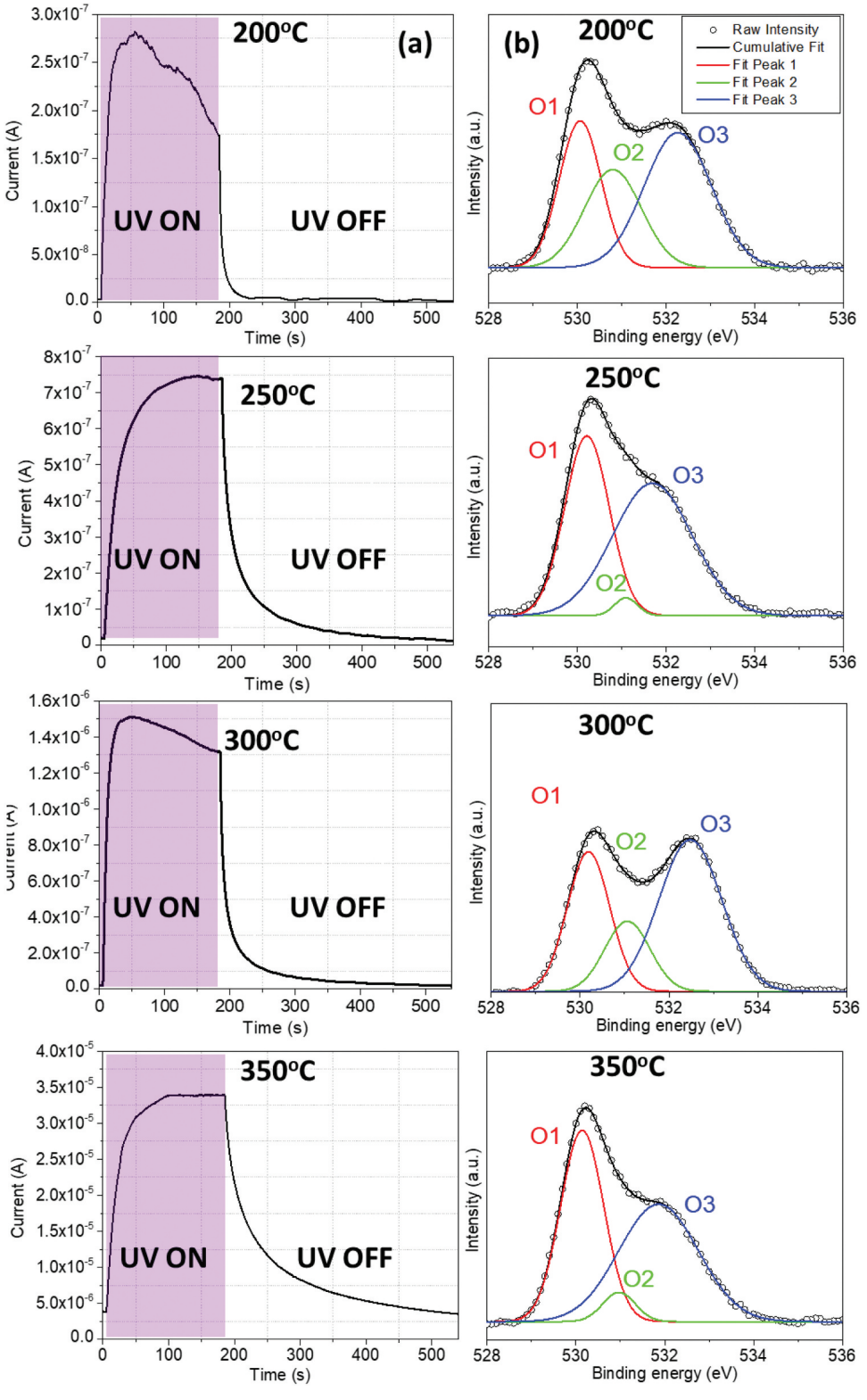

Figure 8. Dynamic response of the printed sensor to UV illumination and fitting by exponential function: (a) response characteristic of sample processed from 200°C to 350°C, respectively. (b) O 1s spectra of printed thin films processed processed at from 200°C to 350°C.

In general, the response time of the printed device to UV illumination is long, which is the result of air desorbing from the surface of the semiconductor due to photo-generated charge carrier. Without UV illumination, oxygen absorbs to ZnO surface by receiving a free electron, causing the lack of charge carrier. Under UV illumination, the generated hole recombines with trapped electron, releasing oxygen and increasing electrical current running through the device [26]. Such air exchanging is the main cause of the long response to UV light of printed device.

The difference in time response characteristics between printed devices with different thermal treatment conditions could be correlated to the surface defects modification as the effect of heating. It is because the transition time of the photodetector reflects the interactions of the semiconductor with ambient air, which are the absorption and desorption of air molecules to the defect sites [46]. Hence, investigating chemical states on the film surface is necessary to understand the photo-response behavior of the printed device.

To evaluate the charge states on the surface of printed films, XPS spectra of the films with a particular focus on the oxygen spectra O1 s are investigated as shown in (Figure 8 (b)). The asymmetric patterns are observed in both samples, which could be deconvoluted to three energy peaks, such as 530.1 eV, 531.0 eV, and 532.4 eV, which are linked to lattice oxygen (O1), oxygen vacancies (O2), and surface oxygen (O3), respectively [47,48].

In general, lattice oxygens of samples processed at 200°C, 250°C, 300°C and 350°C are 33.8%, 36.0%, 24.8% and 41.0%, respectively. Meanwhile, oxygen vacancies slightly change from 26.1% to 31.0%, 24.9% and 25% when higher annealing temperature were applied. Notably, excess oxygen shows a significant variation from 40.1% to 33.1%, 50.3% and 29.0%, according to sample processed at 200°C, 250°C, 300°C and 350°C, respectively. These analyses demonstrate the transformation of excess oxygen to lattice oxygens [48], which is in good agreement with XRD analysis. The reduction of excess oxygen may also lead to less interaction with ambient air, which shows a slower response to UV illumination. In addition, a higher lattice oxygen percentage means that there are more sites are interacting with UV photons and more free charger carriers are generated, which could also promote the photocurrent. Furthermore, at temperature lower than 300°C, the excess oxygen tends to be transformed to oxygen vacancies, while oxygen vacancies tends to be transformed to lattice oxygen due to the filling of free oxygen to the vacancies at a higher temperature. This observation is agreed with previous report which suggested that high processing temperature could widen the gaps of ZnO crystal, hence promote the filling of oxygen atoms to the gaps [48].

Beside the enlargement of the grain size, the thermal annealing of inkjet printed ZnO could help improve the crystal quality. As can be seen in (Figure 7(b)), there is a generally increasing of lattice oxygen, which could benefit the generation of electron-hole under high energy photon and boost the current transportation.

Table 1 presents the comparison of the UV photodetector performance of this work with some representative studies which employ the same polycrystalline thin film of ZnO. It can be seen that in terms of rise time and decay time, this work show comparable performance with films prepared by flame spray pyrolysis approach [49,50], but much slower than those prepare by sol-gel thin film deposition [51,52]. The root cause of this

Table 1. Performance comparison of the ZnO UV photodetectors with polycrystalline thin film structure.

Preparation technique	Light intensity (mW/cm^2)	Bias voltage (V)	Rise time (s)	Decay time (s)	Responsivity (A/W)	I_{ph}/I_{dark}	Ref.
Sol-gel	1.06	120	<0.1	1.3*	61	10^6	[51]
Sol-gel	0.003	5	3.4	5	2.5	1270	[52]
Flame spray pyrolysis	0.1	5	250	150	12	$3.4x10^5$	[49]
Flame spray pyrolysis	0.086	1	145	181	7	$9.3x10^6$	[50]
Inkjet printing	1.08	5	43.1	157.8	33.9	8640	This work

poorer performance could be due to the nature of wrinkling film prepared in this work, which allow more air interaction with the film. This wrinkling structure may also be responsible for the better responsibility of the inkjet printed film as compared to films prepared by flame spray pyrolysis approach.

4. Conclusion

This work studied the electrical characteristics of inkjet-printed ZnO for electrical applications under thermal annealing, which shows a significant responsivity enhancement of more than one thousand times. Band bending at the grain boundaries was also found to be altered by the thermal annealing, which suggests that the annealing might affects the electrical characteristics of the printed film via the band bending modification. Whereby, the merging of grain could lower the barrier between nanoparticles and improve electron mobility. The response characteristics of the semiconductor to UV illumination are also affected by thermal treatment due to the change in surface states as found by XPS analysis. These results provide a fundamental understanding of structural and electrical properties of inkjet-printed semiconductor film using precursor as ink, which is crucial in additive manufacturing of electronic devices.

Acknowledgments

We appreciate the equipment support from Singapore Centre for 3D Printing (SC3DP). We thank Assistant Professor Lau Gih Keong (NTU) for allowing us to use the source metering unit (Agilent B2902A). We thank Associate Professor Fei Duan (NTU) for allowing us to use the tube furnace.

Disclosure statement

No potential conflict of interest was reported by the author(s).

Funding

This work was supported by Nanyang Technological University and the Ministry of Education of Singapore through a Ph.D. Scholarship and AcRF Tier 1 research grant (RG 96/18).

ORCID

Van-Thai Tran http://orcid.org/0000-0002-4799-8934
Yuefan Wei http://orcid.org/0000-0003-3050-1589
Hejun Du http://orcid.org/0000-0002-6204-7520

References

[1] Lewis JA. Direct ink writing of 3d functional materials. Adv Funct Mater. 2006;16 (17):2193–2204.
[2] Choi HW, Zhou T, Singh M, et al. Recent developments and directions in printed nanomaterials. Nanoscale. 2015;7(8):3338–3355.
[3] Zhan Z, An J, Wei Y, et al. Inkjet-printed optoelectronics. Nanoscale. 2017;9(3):965–993.
[4] Ko SH, Pan H, Grigoropoulos CP, et al. Air stable high resolution organic transistors by selective laser sintering of ink-jet printed metal nanoparticles. Appl Phys Lett. 2007 April 02;90(14):141103.
[5] Ko SH, Pan H, Grigoropoulos CP, et al. All-inkjet-printed flexible electronics fabrication on a polymer substrate by low-temperature high-resolution selective laser sintering of metal nanoparticles. Nanotechnology. 2007 August 01;18(34):345202.
[6] Ko SH, Pan H, Grigoropoulos CP, et al. Lithography-free high-resolution organic transistor arrays on polymer substrate by low energy selective laser ablation of inkjet-printed nanoparticle film. Appl Phys A. 2008 August 01;92(3):579–587.
[7] Li D, Lai W-Y, Zhang Y-Z, et al. Printable Transparent Conductive Films for Flexible Electronics. Adv Mater. 2018 March 01;30(10):1704738. DOI:10.1002/adma.201704738
[8] Zhou L, Chen X, Su W, et al. In-depth investigation of inkjet-printed silver electrodes over large-area: ink recipe, flow, and solidification. Adv Mater Interfaces. 2102548. 2022; March 15. DOI:10.1002/admi.202102548.
[9] Zhou L, Yu M, Yao L, et al. Mayer rod-coated organic light-emitting devices: binary solvent inks, film topography optimization, and large-area fabrication. Adv Eng Mater. 2101558. 2022; February 25. DOI:10.1002/adem.202101558.
[10] Zhou L, Yu M, Chen X, et al. Screen-Printed poly(3,4-ethylenedioxythiophene):poly-(styrenesulfonate) grids as ito-free anodes for flexible organic light-emitting diodes. Adv Funct Mater. 2018 March 01; 28(11): 1705955.
[11] Lavery LL, Whiting GL, Arias AC. All ink-jet printed polyfluorene photosensor for high illuminance detection. Organic Electron. 2011;12(4):682–685, 4//.
[12] Jung S, Sou A, Banger K, et al. All-inkjet-printed, all-air-processed solar cells. Adv Energy Mater. 2014;4(14):1400432.
[13] Pace G, Grimoldi A, Natali D, et al. All-organic and fully-printed semitransparent photodetectors based on narrow bandgap conjugated molecules. Adv Mater. 2014;26(39):6773–6777.
[14] Liang YN, Lok BK, Wang L, et al. Effects of the morphology of inkjet printed zinc oxide (ZnO) on thin film transistor performance and seeded ZnO nanorod growth. Thin Solid Films. 2013 January 10;544:509–514.
[15] Lu J., Wang, W., Liang, J. Contact resistance reduction of low temperature atomic layer deposition zno thin film transistor using ar plasma surface treatment. *IEEE Electron Device Letters*. pp. 1, 2022; 10.1109/LED.2022.3169345.
[16] Tran V-T, Wei Y, Yang H, et al. All-inkjet-printed flexible ZnO micro photodetector for a wearable UV monitoring device.Nanotechnology. 2017;28(9):095204.
[17] Tang J-F, Sie Y-D, Tseng Z-L, et al. Perovskite quantum Dot–ZnO nanowire composites for ultraviolet–visible photodetectors. ACS Appl Nano Mater. 2022 April 23;5(5):7237–7245.
[18] Sanchez JG, Balderrama VS, Garduño SI, et al. Impact of inkjet printed ZnO electron transport layer on the characteristics of polymer solar cells. RSC Adv. 2018;8(24):13094–13102.

[19] Tsarev S, Olthof S, Boldyreva AG, et al. Reactive modification of zinc oxide with methylammonium iodide boosts the operational stability of perovskite solar cells. Nano Energy. 2021 May 01;83: 105774.
[20] Haghayegh F, Salahandish R, Hassani M, et al. Highly stable buffer-based zinc oxide/reduced graphene oxide nanosurface chemistry for rapid immunosensing of SARS-CoV-2 antigens. ACS Appl Mater Interfaces. 2022 March 02;14(8):10844–10855.
[21] Ko SH, Lee D, Hotz N, et al. Digital selective growth of ZnO nanowire arrays from inkjet-printed nanoparticle seeds on a flexible substrate. Langmuir. 2012 March 13;28 (10):4787–4792.
[22] Kwon J, Hong S, Lee H, et al. Direct selective growth of ZnO nanowire arrays from inkjet-printed zinc acetate precursor on a heated substrate. Nanoscale Res Lett. 2013 November 20;8(1):489.
[23] Zhang Z, Yates JT. Band bending in semiconductors: chemical and physical consequences at surfaces and interfaces. Chem Rev. 2012 October 10;112(10):5520–5551.
[24] Greuter F, Blatter G. Electrical properties of grain boundaries in polycrystalline compound semiconductors.Semicond Sci Technol. 1990;5(2):111.
[25] Chen C-Y, Retamal JRD, Wu I-W, et al. Probing surface band bending of surface-engineered metal oxide nanowires. ACS Nano. 2012 November 27;6(11):9366–9372.
[26] Liu X, Gu L, Zhang Q, et al. All-printable band-edge modulated ZnO nanowire photodetectors with ultra-high detectivity. *Nat Commun*, Article. 5: 06 May 2014. DOI:10.1038/ncomms5007.
[27] Gedamu D, Paulowicz I, Kaps S, et al. Rapid fabrication technique for interpenetrated ZnO nanotetrapod networks for fast UV Sensors. Adv Mater. 2014;26(10):1541–1550.
[28] Liu Q, Gong M, Cook B, et al. Fused nanojunctions of electron-depleted zno nanoparticles for extraordinary performance in ultraviolet detection. Adv Mater Interfaces. 2017;4(6):1601064.
[29] Pan H, Misra N, Ko SH, et al. Melt-mediated coalescence of solution-deposited ZnO nanoparticles by excimer laser annealing for thin-film transistor fabrication. Appl Phys A. 2009 January 01;94(1):111–115.
[30] Lee D, Pan H, Ko SH, et al. Non-vacuum, single-step conductive transparent ZnO patterning by ultra-short pulsed laser annealing of solution-deposited nanoparticles. Appl Phys A. 2012 April 01;107(1):161–171.
[31] Hosono E, Fujihara S, Kimura T, et al. Growth of layered basic zinc acetate in methanolic solutions and its pyrolytic transformation into porous zinc oxide films. J Colloid Interface Sci. 2004 April 15;272(2):391–398.
[32] Ryu SY, Seo JH, Hafeez H, et al. Effects of the wrinkle structure and flat structure formed during static low-temperature annealing of ZnO on the performance of inverted polymer solar cells. J Phys Chem C. 2017 May 04;121(17):9191–9201.
[33] Bu IYY. Sol–gel production of ZnO:CO: effect of post-annealing temperature on its optoelectronic properties. Mater Sci Semicond Process. 2016;41:240–245, 1//.
[34] Justin Raj C, Karthick SN, Hemalatha KV, et al. Synthesis of self-light-scattering wrinkle structured ZnO photoanode by sol–gel method for dye-sensitized solar cells. *Appl Phys A* j article. 2014;116(2):811–816.
[35] Led D, Pillai SC, Watson GW, et al. Microwave induced preparation of a-axis oriented double-ended needle-shaped ZnO microparticles. Chem Comm. 2004;10(20):2294–2295.
[36] Khorsand Zak A, Abd WH, Majid MEA, et al. X-ray analysis of ZnO nanoparticles by Williamson–Hall and size–strain plot methods. Solid State Sci. 2011;13(1):251–256, 1//.
[37] Demoisson F, Piolet R, Bernard F. Hydrothermal synthesis of ZnO crystals from Zn(OH)2 metastable phases at room to supercritical conditions. Cryst Growth Des. 2014 November 05;14(11):5388–5396.
[38] McBride RA, Kelly JM, McCormack DE. Growth of well-defined ZnO microparticles by hydroxide ion hydrolysis of zinc salts. J Mater Chem. 2003;13(5):1196–1201.
[39] Dhar S, Majumder T, Mondal SP. Graphene quantum dot-sensitized ZnO nanorod/polymer schottky junction uv detector with superior external quantum efficiency, detectivity, and responsivity. ACS Appl Mater Interfaces. 2016 November 23;8(46):31822–31831.

[40] Baccarani G, Riccò B, Spadini G. Transport properties of polycrystalline silicon films. J Appl Phys. 1978;49(11):5565–5570.
[41] Gelderman K, Lee L, Donne SW. Flat-band potential of a semiconductor: using the mott–schottky equation. J Chem Educ. 2007 April 01;84(4):685.
[42] Windisch CF, Exarhos GJ. Mott–Schottky analysis of thin ZnO films. J Vac Sci Technol A. 2000 July 01;18(4):1677–1680.
[43] Allagui A, Alawadhi H, Alkaaby M, et al. Mott–Schottky analysis of flower-like ZnO micro-structures with constant phase element behavior. Phys Status Solidi A. 2016;213(1):139–145.
[44] Ren L, Tian T, Li Y, et al. High-Performance UV photodetection of unique ZnO nanowires from zinc carbonate hydroxide nanobelts. ACS Appl Mater Interfaces. 2013 June 26;5 (12):5861–5867.
[45] Yang LL, Zhao QX, Willander M, et al. Effective suppression of surface recombination in ZnO nanorods arrays during the growth process. Cryst Growth Des. 2010 April 07;10(4):1904–1910.
[46] Panda SK, Jacob C. Preparation of transparent ZnO thin films and their application in UV sensor devices. Solid-State Electron. 2012;73:44–50.
[47] Meena JS, Chu M-C, Chang Y-C, et al. Effect of oxygen plasma on the surface states of ZnO films used to produce thin-film transistors on soft plastic sheets. J Mater Chem C. 2013;1 (40):6613–6622.
[48] Jiang L, Li J, Huang K, et al. Low-temperature and solution-processable Zinc oxide transistors for transparent electronics. ACS Omega. 2017 December 31;2(12):8990–8996.
[49] Nasiri N, Bo R, Wang F, et al. Ultraporous electron-depleted ZnO nanoparticle networks for highly sensitive portable visible-blind UV photodetectors. Adv Mater. 2015;27(29):4336–4343.
[50] Noushin N, Renheng B, Hongjun C, et al. Structural engineering of nano-grain boundaries for low-voltage UV-photodetectors with gigantic photo- to dark-current ratios. Adv Opt Mater. 2016;4(11):1787–1795.
[51] Jin Y, Wang J, Sun B, et al. Solution-Processed ultraviolet photodetectors based on colloidal ZnO nanoparticles. Nano Lett. 2008 June 01;8(6):1649–1653.
[52] Qingfeng L, Gong M, Cook B, et al. Oxygen plasma surface activation of electron-depleted ZnO nanoparticle films for performance-enhanced ultraviolet photodetectors. Phys Status Solidi A. 2017;214(11):1700176.